Cohesive-Zone Modeling of the Deformation and Fracture of Weld-Bonded Joints

Two cohesive-fracture parameters were developed, then combined to predict the behavior of weld-bonded geometries

M. N. CAVALLI, M. D. THOULESS, AND Q. D. YANG

ABSTRACT. In previous work, cohesive-zone models have been developed separately for the analysis of adhesively bonded joints and for the analysis of spot welded joints. The appropriate fracture parameters have been determined for a commercial rubber-toughened epoxy for bonding thin sheets of 5754 aluminum alloy. Fracture parameters have also been determined for spot welds formed under specific processing conditions with this same alloy. It has been established that these parameters provide a predictive capability for design, in the sense that loads, deformation, and energy absorption can be consistently predicted for different geometries of joints bonded under nominally identical conditions. In the present paper, these two separate models are combined to provide a design tool for weld bonding in which adhesive technology is combined with spot welding. It is demonstrated that the models developed separately for the two joining techniques can be combined and used with no further modification to predict the behavior of weld-bonded geometries. In particular, the strength and energy-absorption characteristics of a joint from initial loading through final failure are reproduced for the two different geometries investigated.

Introduction

Concerns about fuel economy, safety, reliability, and performance are continually driving automotive designers and engineers to incorporate new materials, structures, and techniques into their designs. One technique that is receiving increased attention is weld bonding: a joining process that combines resistance spot welding with a layer of structural adhesive in a single joint (Ref. 1). Various advantages of weld-bonded joints over joints formed only by spot welding or only by adhesive bonding are driving the interest. Weld-bonded joints have been shown to be stronger than joints made by either spot welding or adhesive bonding alone (Refs. 2–12). Furthermore, the presence of a continuous adhesive layer increases the stiffness (Refs. 9, 10) and fatigue resistance of a spot-welded joint (Refs. 9–12), while possible time-dependent or temperature-dependent deterioration of the adhesive can be at least partially mitigated by the presence of spot welds (Refs. 9, 11). These advantages of weld-bonded joints offer the potential for stronger, safer automotive structures.

To utilize the full potential of weld-bonded joints in automotive structures, analytical tools must be developed to predict their deformation and fracture. Current knowledge of the behavior of weld-bonded joints is primarily phenomenological in nature, and is typically concerned with the effect of welding and joint parameters on joint strength. Experimental studies have been conducted to explore the effect of welding parameters on nugget size (Refs. 2, 5, 8), the effect of nugget size on joint strength (Ref. 5), the effect of nugget expulsion on joint strength (Ref. 10), and the effect of weld density on joint strength (Refs. 4, 7). Further experimental work has investigated the effect of joint width on joint strength (Ref. 3), the effect of environmental conditions on strength and fatigue properties (Refs. 6, 9, 11), and the effect of loading rate on joint strength and energy absorption (Ref. 6). Finite-element methods have been used to compare the distribution of stresses in spot-welded, adhesively bonded, and weld-bonded joints (Refs. 13–15). General trends in weld-bonded joint behavior have been established as a result of these previous studies. However, a method for predicting the deformation and fracture of weld-bonded joints has not yet been established.

KEY WORDS

Cohesive-Zone Models
Adhesively Bonded Joints
Spot Welded Joints
Aluminum Alloy 5754
Weld-Bonded Joints
Deformation Fracture

Several failure criteria have been proposed to predict the failure loads of spot-welded joints. These criteria are typically based on the idea that a single parameter (e.g., a critical stress or force) is sufficient to describe the failure of spot-welded joints subjected to a single mode of loading. Combining the parameters for each mode permits mixed-mode criteria to be developed. For example, Lee et al. (Ref. 16) proposed a mixed-mode criterion of the form

$$\left(\frac{S_n}{S_{nu}}\right)^n + \left(\frac{S_s}{S_{su}}\right)^n = 1 \qquad (1A)$$

where S_n and S_s are the applied normal and shear forces, S_{nu} and S_{su} are the normal and shear strengths of the weld, and n is an experimental fitting parameter. An analytical approach to modeling the onset of yield at the circumference of a weld results in this same criterion, with $n = 2$ (Ref. 17). Wung (Ref. 18) and Wung et al. (Ref. 19) also used a strength model but assumed that there are four fundamental modes of applied loading: 1) a normal force, f_n, 2) a shear force, f_s, 3) a bending moment, m_b, and 4) a torque, m_t. It was shown that if the failure parameter for each individual mode is given by F_n, F_s, M_b, and M_t, with failure being defined as the linear limit of the load-deflection curve, a mixed-mode failure criterion of the form

$$\left(\frac{f_n}{F_n}\right)^\alpha + \left(\frac{f_s}{F_s}\right)^\beta + \left(\frac{m_b}{M_b}\right)^\gamma + \left(\frac{m_t}{M_t}\right)^\beta = 1 \qquad (1B)$$

where α, β, γ, and δ are empirical parameters that are determined experimentally, can be used.

Most recently, the current authors

M. N. CAVALLI is with the Department of Mechanical Engineering, and M. D. THOULESS is with the Department of Materials Science and Engineering, University of Michigan, Ann Arbor, Mich. Q. D. YANG is with Rockwell Scientific Co., Thousand Oaks, Calif.

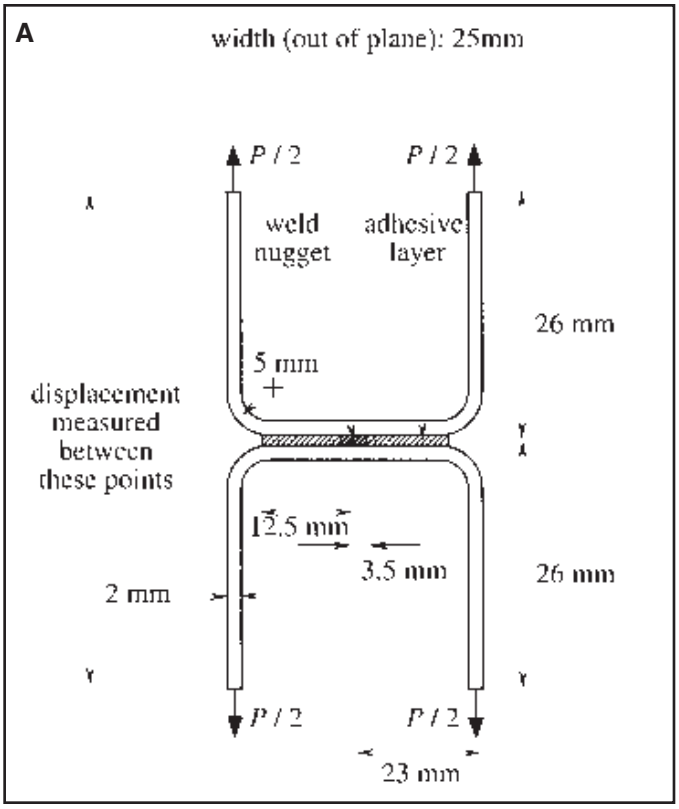

Fig. 1 — The shape and dimensions of joints used in this study. A — Weld-bonded coach-peel; B — lap-shear weld-bonded joints.

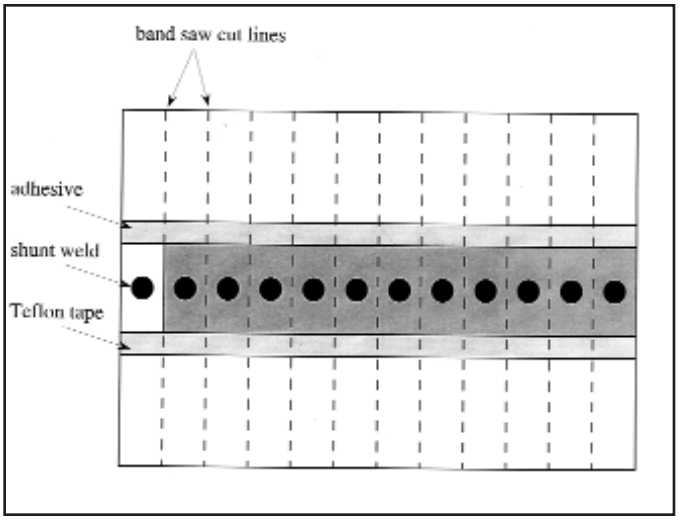

Fig. 2 — Sheets of 10–12 specimens were spot welded and cured together. The individual specimens were then cut apart and, in the case of coach-peel samples, formed into the appropriate shape. The first spot weld in each batch was a shunt weld, with no adhesive between the metal sheets.

have proposed using a cohesive-zone approach for modeling the deformation and fracture of spot-welded joints (Refs. 20, 21). Cohesive-zone models essentially introduce both an energy and strength parameter into the description of fracture, since the necessity of such a two-parameter model to describe crack propagation when small-scale yielding conditions are not appropriate is well documented (Refs. 22–29). The current authors demonstrated that once the appropriate cohesive parameters for a particular weld have been properly characterized, numerical modeling can be used to produce predictions of the strength, energy absorption, and failure mechanism for different geometries containing a nominally similar weld. The major advantages of this approach are that it enables automatic prediction of the failure mechanism (nugget fracture or weld pullout) and full load-deflection curves for arbitrary joint geometries (Refs. 20, 21). Similar predictive capabilities of cohesive-zone models have also been demonstrated for adhesive joints (Refs. 26–31). It is the intent of the current work to investigate whether the cohesive models for an adhesive can be combined with cohesive models for a weld to predict the behavior of weld-bonded joints. To this end, the present work combines an adhesive and welds that are nominally identical to those used separately in the previous studies (Refs. 20, 21, 26–31), so that the cohesive models for each joining technique can be used without modification in modeling the weld-bonded structures. Predictions based on these models are then compared to experimental results.

Specimen Preparation and Testing

Both coach-peel and single-lap-shear weld-bonded joints were used for this study — Fig. 1. The specimens were fabricated from 2-mm-thick 5754-O aluminum sheets using a commercial toughened epoxy adhesive.[1] This non-heat-treatable aluminum alloy was chosen to avoid possible complications associated with any heat-affected zone. The alloy and surface treatments prior to bonding were identical to those used in the earlier studies of the adhesive alone. Strips of Teflon® tape were used to define the boundaries of the bonded region, and 0.25-mm glass beads were added to the uncured adhesive to ensure uniform thickness of the adhesive layer. The weld-bonded specimens were fabricated using the "weld-through" technique; i.e., the adhesive was applied, resistance spot welds were made through the uncured adhesive layer, and then the adhesive was cured at 180°C for 45 min. It was found to be extremely difficult to produce individual specimens in this manner because an initial current path between the electrodes is needed to prevent arcing. Limited experiments were made with increased welding pressure and ramping of the weld current, but arcing was still observed. To overcome this problem, 10–12 welds were made on a large sheet, with one of the welds being a shunt weld with no adhesive — Fig. 2. After welding and curing, individual specimens were cut from these sheets. The coach-peel specimens were then bent into shape. This bending process resulted in some inconsistencies in the geometry of the coach-peel specimens. It may have contributed to the greater variability in the load-displacement curves that was subsequently observed for the coach-peel specimens than for the lap-shear specimens.

All the specimens were welded using a

1. XD4601 (Ciba-Geigy)

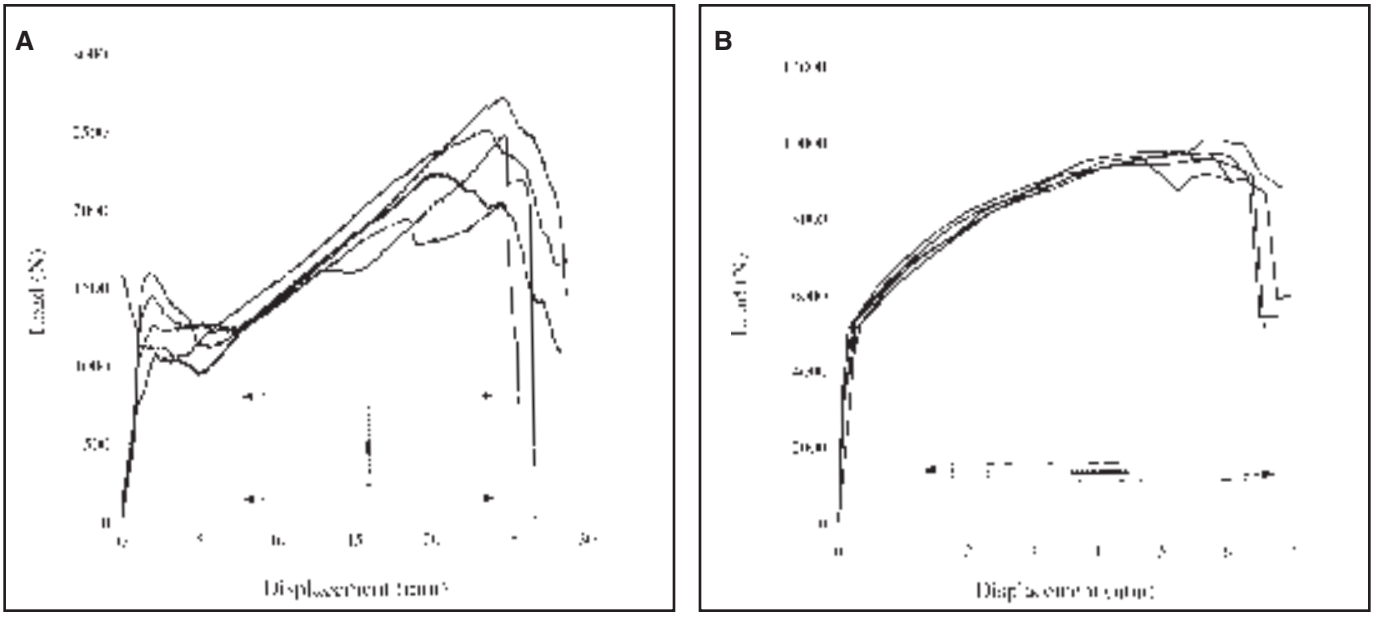

Fig. 3 — A series of experimental load-displacement curves. A — The weld-bonded coach-peel specimens with the geometry shown in Fig. 1A; B — the weld-bonded lap-shear specimens with the geometry shown in Fig. 1B.

square waveform welding current of 23 kA for 17 cycles. The electrodes were in the shape of truncated cones with tip diameters of 8 mm. The resulting nugget diameters were 7 ± 1 mm for all specimens. It is emphasized that both the adhesive bonding and the spot welding processes were nominally identical to the processes used to prepare specimens for the evaluation of the cohesive parameters in the earlier studies (Refs. 20, 21, 26-30). The specimens were tested in a screw-driven tensile-testing machine at a displacement rate of 5 mm/min for the coach-peel specimens, and at a displacement rate of 0.5 mm/min for the lap-shear specimens. These rates were comparable to those used in the earlier work. A CCD camera was used to record the relative displacements of the points where the load was applied for both geometries.

Figure 3A and B shows a series of load-displacement curves for the coach-peel and lap-shear specimens, respectively. The data for the coach-peel geometry characteristically has two maxima; the initial peak in Fig. 3A represents the start of crack propagation within the adhesive, and the second maximum corresponds to failure of the weld and remaining adhesive ligament. In this geometry, failure occurred by pullout of the weld nugget and interfacial fracture of the adhesive layer. The shapes of the curves for the lap-shear geometry is rather different in that there is no characteristic peak associated with crack initiation within the adhesive layer. This is similar to what has been observed for lap-shear joints with adhesive bonding only (Refs. 29, 30). While some specimens behaved in the expected symmetrical fashion with interfacial cracking beginning almost simultaneously from both ends of the adhesive layer, other specimens behaved asymmetrically with an interfacial crack propagating from one end to almost halfway across the specimen, before a second interfacial crack began to advance from the other end. As the adhesive failed, and the adherend deformed, the load continued to increase as the crack progressed toward the weld nugget. At the peak load, the weld had not yet failed; final failure of the nugget appeared to occur after a catastrophic load drop following the peak load. It is believed that the larger range of uncertainty observed for the coach-peel specimens than for the lap-shear specimens may be partially associated with the variation in geometry caused by shaping done after the welding process. The sizes of the welds were essentially identical for all specimens tested (7 ± 1 mm), and there was no systematic effect of location in the original sheet or of the weld size on the observed properties. It was also observed that slight asymmetries in the geometry of the coach-peel specimens led to some twisting during testing, which may also have been responsible for variations in the load-displacement behavior.

Cohesive-Zone Modeling

Essentially all that was done in the numerical modeling aspects of this paper was to combine the separate models previously developed for adhesive and welded systems. The materials and welding schedules used in the present work were nominally identical to those used previously, and the material properties that had previously been determined, including cohesive parameters, were used without modification in the numerical portion of this work. Details of the numerical modeling, and of how the properties were determined, can be found in those earlier works (Refs. 20, 21, 25–30). Therefore, only a brief summary of the techniques and properties are provided in this paper.

All finite-element calculations were performed using the *ABAQUS* commercial software package (version 6.3). The calculations were fully 3-D, but three nominal planes of symmetry allowed a one-eighth model to be used for the coach-peel geometry, while a single plane of symmetry allowed a one-half model to be used for the lap-shear geometry.[2] The geometries of the specimens used for the numerical calculations were identical to those of the fabricated specimens, and the aluminum adherends were modeled using 8-noded continuum elements with properties determined from tensile tests (Ref. 32). Isotropic yielding with a von Mises yield criterion and power-law hardening were assumed. Young's modulus, E, of the aluminum was 69 ± 5 GPa, the yield stress, σ_y, was 113 ± 3 MPa, Poisson's ratio was taken to be 0.3, and the power-law hardening was of the form

$$\sigma = A\varepsilon^n \qquad (2)$$

2. The assumption of symmetry for the coach peel geometry ignored the possibility of assymmetrical fabrication; some effects of asymmetry were observed during testing.

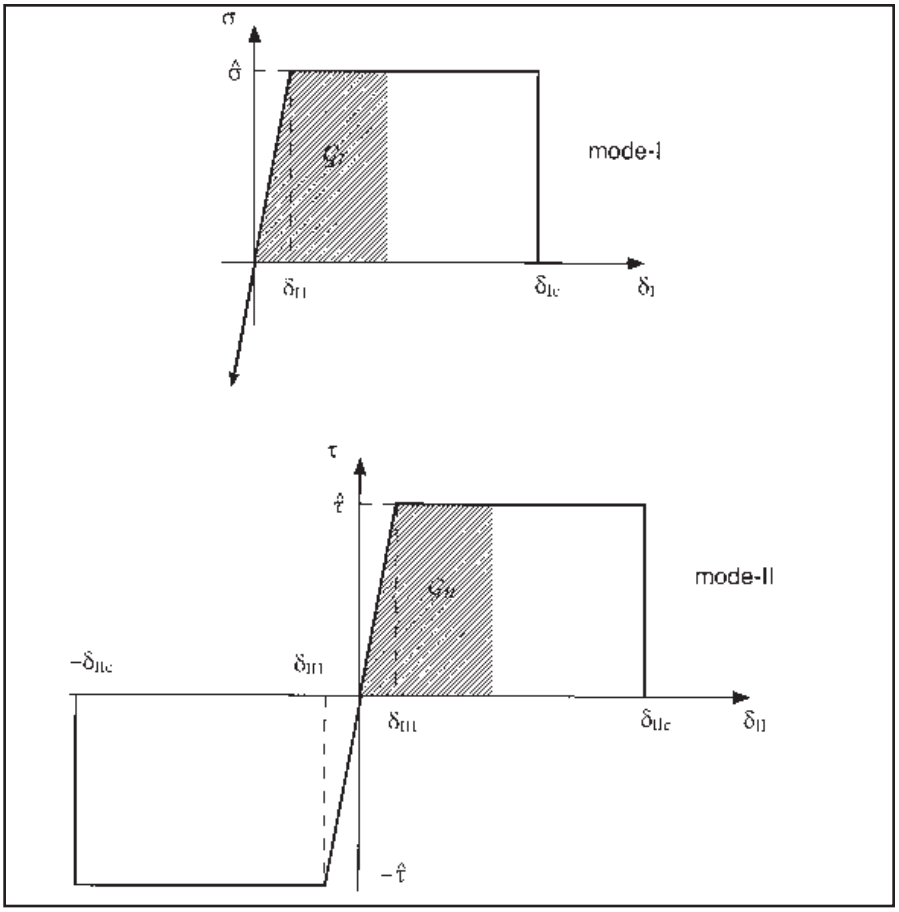

Fig. 4 — For each mode of loading, tractions between the nodes of each user-defined element obey a traction-separation law of the form seen here. The area under the curve represents the material toughness under single-mode loading. (From Ref. 20.)

where A = 494 ± 6 MPa and n = 0.3 ± 0.01. Uncertainties in the material properties and the dimensions of the fabricated specimens were incorporated in sensitivity studies of the predictions.

Fracture was incorporated into the numerical models by the use of cohesive zones in any region where fracture was expected to occur. These cohesive zones consisted of user-defined elements, with a characteristic traction-separation law appropriate for the local region. The adhesive region was modeled with cohesive elements that captured the interfacial fracture behavior of the adhesive (Ref. 29), the weld-nugget region was modeled with cohesive elements that captured the fracture behavior of the nugget (Refs. 20, 21), and the region in the adherends around the nugget was modeled with cohesive elements that captured the pullout behavior of the nugget (Refs. 20, 21). All potential failure mechanisms were allowed to evolve naturally in the calculations. No assumptions were made *a priori* about the failure. As in the earlier work, both the adhesive layer and the nugget between the adherends were completely replaced by cohesive elements. It should be noted that the area over which the cohesive elements acted was varied to correspond with the experimentally observed range of weld sizes. This variation is reflected in the results that will be presented in the following section. The cohesive laws that controlled the fracture behavior in the three different regions were assumed to be trapezoidal in form, as indicated in Fig. 4. A separate law was assumed for each mode of deformation in each failure location. Only mode-I and mode-II (normal and in-plane shear) failure were considered for the adhesive and nugget. However, weld pullout occurs by a combination of modes I, II, and III (out-of-plane shear), and the mode II and mode III cohesive laws for pullout were assumed to be identical. The two important parameters of these cohesive laws are the peak strength and the toughness. These were taken from the earlier work and are listed in Table 1.[3] It should be emphasized that a key aspect of this paper is the incorporation of weld and adhesive cohesive properties determined separately and then used without modification to model weld-bonded geometries.

As in the previous work on adhesive bonding and spot-weld bonding, a simple mixed-mode failure criterion of the form (Refs. 20, 28, 29)

$$\frac{G_I}{\Gamma_I}+\frac{G_{II}}{\Gamma_{II}}+\frac{G_{III}}{\Gamma_{III}}=1 \qquad (3)$$

was assumed, where G_I, G_{II}, and G_{III} represent the energy-release rates for each mode (the area under the curve up to the applied displacement, see Fig. 4), and Γ_I, Γ_{II}, and Γ_{III} represent the total area under the traction-separation curve for each mode. The numerical calculations progressed by allowing the node pairs of the cohesive element to deform according to the appropriate traction-separation law. Equation 3 was evaluated at each numerical increment to determine if the failure criterion of a node pair was met. If it had not been met anywhere, then the calculations continued; if it had been met, the load-bearing capabilities of the affected node-pair were removed and the numerical conditions reevaluated before the calculations continued.

Results

Figure 5A compares the predicted behavior of coach-peel joints that have been weld-bonded, spot welded only, and adhesively bonded only. These numerical predictions were calculated using the average cohesive-zone parameters for the weld and adhesive given in Table 1, and the dimensions given in Fig. 1A. The numerical results indicated that failure of the weld occurred by pullout for both the weld-bonded and spot welded configurations. Again, it should be emphasized that the possibility of both failure modes of nugget fracture and weld pullout were allowed in the numerical calculations; however, the calculations evolved to a failure mode of weld pullout, as observed experimentally. Figure 5A shows that, in this geometry, weld bonding gives the advantage of adhesive bonding at low loads, in that the stiffness and yield load are dramatically higher than for the same geometry bonded

3. A Ciba-Geigy adhesive designated as XD4600 was used in previous work. The designation of the adhesive available for this work (XD4601) was slightly different, so there was some concern that the cohesive-zone parameters might have changed. However, wedge tests (Refs. 26, 31) confirmed that the mode-I properties were unchanged within experimental uncertainty, so the previously published values for both the mode-I and mode-II properties were used without modification in this work. Interfacial fracture was always observed for the adhesive; so the interfacial values of the cohesive-zone parameters were used in this paper.

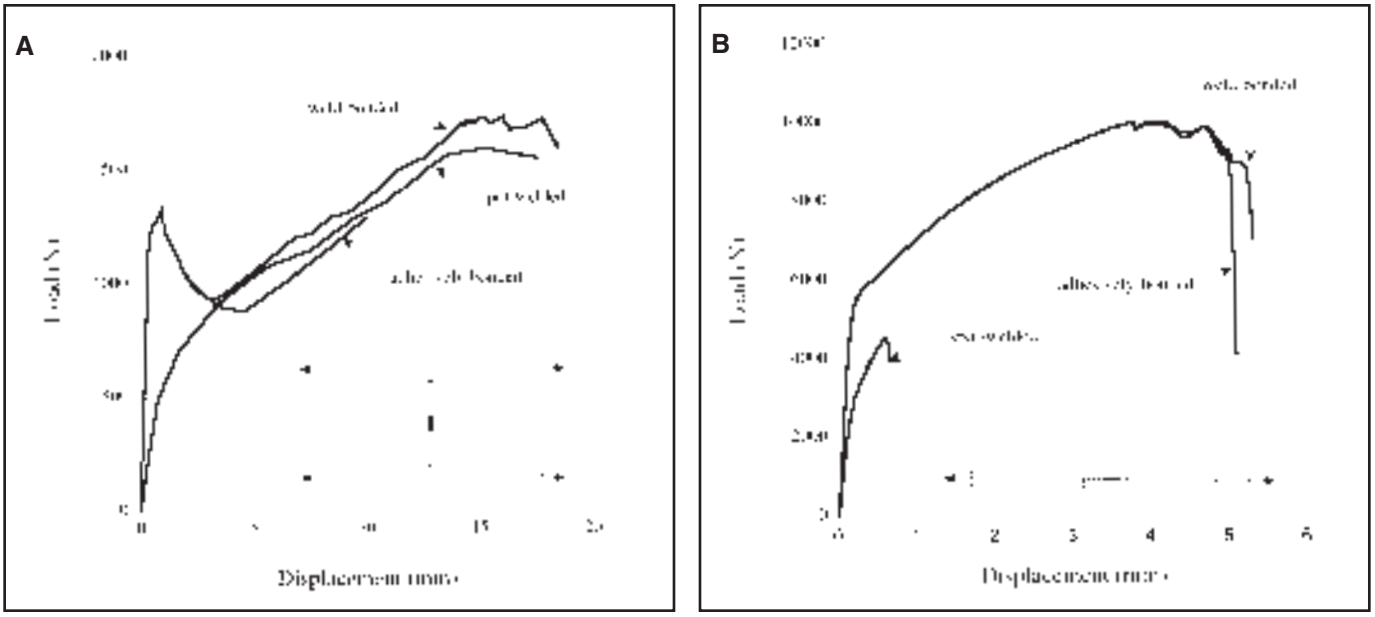

Fig. 5 — A comparison between the behaviors of the following: A — Weld-bonded, spot-welded, and adhesively bonded coach-peel joints with dimensions indicated by Fig. 1A; and B — weld-bonded, spot-welded, and adhesively bonded lap-shear joints with dimensions indicated by Fig. 1B. The nugget diameters for the spot-welded and weld-bonded joints were assumed to be 7.0 mm, and all cohesive properties were assumed to be the average of the values given in Table 1.

by a single spot weld. This is because the initial stiffness of the coach-peel geometry is dominated by bending of the arms if there is only a single spot weld. The presence of an adhesive layer between the arms suppresses this bending. Bending can occur when the adhesive fractures and, consequently, the load drops as a crack propagates through the adhesive. During this stage of deformation, the spot weld does not appear to play a significant role on the load-bearing capacity of the joint, and the weld-bonded joint behaves identically to the adhesively bonded joint. After a crack has propagated most of the way through a coach-peel specimen, it begins to behave like a butt joint as the last ligament of adhesive carries all the applied load. The load therefore increases in this stage of the process, until final catastrophic failure of the adhesive occurs. In a weld-bonded joint, the spot weld contributes to the load-bearing capability in this regime. As a result, the load is supported by both the spot weld and the adhesive until final failure. Since catastrophic failure of the adhesive is inhibited by the presence of the spot weld, a small ligament of adhesive is maintained until final fracture of the weld, and the overall load-bearing capability of a weld-bonded joint is slightly higher than that of a spot-welded joint. Overall, the weld-bonded geometry behaves as an aggregate of the weld and of the adhesive bond, with the adhesive dominating at low displacements and the spot weld dominating at large displacements. The major advantages of weld bonding in this geometry are an enhanced stiffness and more resistance to yield; this, in turn, translates to some overall improvement in energy absorption.

Table 1 — Cohesive-Zone Parameters Used in the Numerical Modeling of the Weld-Bonded Joint

	Mode I		Mode II	
	Strength (MPa)	Toughness (kJ · m^{-2})	Strength (MPa)	Toughness (kJ · m^{-2})
Nugget fracture	$\widehat{\sigma}_N = 290 \pm 20$	$\Gamma_{IN} = 13 \pm 2$	$\widehat{\tau}_N = 200 \pm 20$	$\Gamma_{IIN} = 26 \pm 4$
Weld pullout	$\widehat{\sigma}_P = 340 \pm 10$	$\Gamma_{IP} = 13 \pm 2$	$\widehat{\tau}_P = 230 \pm 10$	$\Gamma_{IIP} = 26 \pm 4$
Adhesive fracture	$\widehat{\sigma}_A = 60 \pm 10$	$\Gamma_{IA} = 1.0 \pm 0.15$	$\widehat{\tau}_A = 35 \pm 5$	$\Gamma_{IIA} = 5.4 \pm 0.8$

Figure 5B shows a comparison between lap-shear joints formed by an adhesive, a single spot weld, and a combination of the two bonding techniques. For the material properties considered, the spot-welded configuration results in much lower failure loads and displacements than are obtained with the configuration bonded with an adhesive only. As a result, upon combining the two techniques, the properties of the lap-shear are dominated by the adhesive almost the whole way to final failure. Only when the adhesive has almost completely failed does the spot weld start influencing the behavior, giving a slightly extended critical displacement before the onset of final failure. In contrast to the results shown in Fig. 5A, the numerical simulations indicated that final failure of the weld occurs by nugget fracture in this geometry. However, in the weld-bonded configuration, the nugget has not completely fractured at the peak load. A failure instability occurs before final fracture of the nugget. This is consistent with the experimental observations discussed in the previous section, and may be associated with the fact that the strength of the weld-bonded lap-shear specimen is much greater than the strength of the lap-shear specimen with a single spot weld.

Figure 6A shows a comparison between the experimentally measured load-displacement response of the weld-bonded coach-peel joints and the numerically predicted behavior. Figure 6B shows a comparison between the experimentally measured load-displacement response of the weld-bonded lap-shear joints and the numerically predicted behavior. As discussed above, pullout of the weld occurred in the coach-peel specimens for both the experimental and numerical results, whereas nugget failure was predicted numerically and observed experimentally for the lap-shear geometry. It will be observed that the numerical calculations capture the intricacies of the

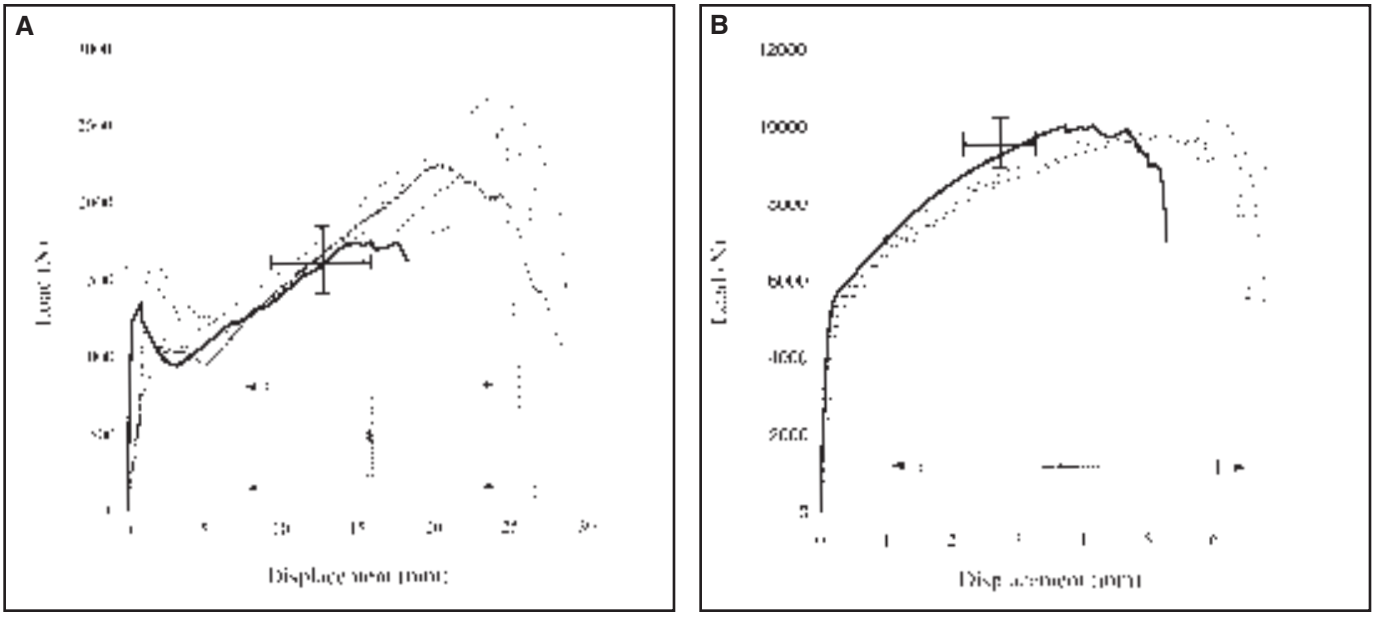

Fig. 6 — A comparison between experimental results and numerical predictions for the following: A — The weld-bonded coach-peel joints; B — the weld-bonded lap-shear joints. The dotted lines correspond to the experimental results shown earlier in Fig. 3A and B. The solid lines indicate the numerical predictions based on the cohesive-zone parameters of Table 1. The uncertainty for the numerical results indicates the effect of the variability of input parameters associated with the geometry including the size of the weld, the material properties of the aluminum, the cohesive parameters of the weld, and the geometry.

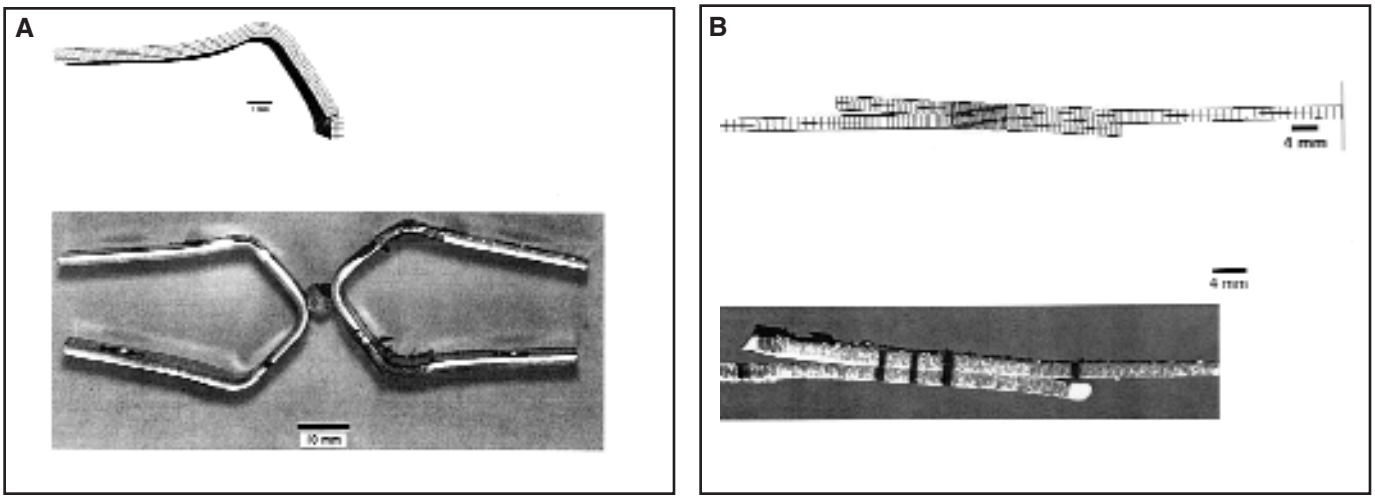

Fig. 7 — A comparison of the deformed shapes predicted by the numerical calculations and those observed experimentally for the following: A — the weld-bonded coach-peel joint; B — the weld-bonded lap-shear joint.

load-displacement curves, including consistent predictions for both the loads and displacements. For the coach-peel geometry, the numerical predictions include both the initial peak associated with adhesive cracking and the final peak associated with failure of the weld. As an aside, it should be noted that the geometry used to determine the mode-I cohesive parameters of the adhesive was unrelated to this coach-peel geometry (Refs. 26, 29), and even the coach-peel geometry used to determine the mode-I pullout parameters for the weld (Refs. 20, 21) had different dimensions from that used in the present study. Therefore, the agreement between the numerical predictions and the experimental results is particularly satisfying. A similar agreement is seen between the numerical predictions and the experimental observations for the lap-shear geometry. The numerical model predicts the steady rise in applied load associated with adhesive failure up to the peak load observed experimentally. Comparisons of the deformed experimental geometries with the final shapes predicted by the numerical calculations are shown for both geometries in Fig. 7A, B. Again, good agreement is seen for both geometries.

The results show that cohesive-zone modeling can predict the quasi-static load-displacement behavior of weld-bonded joints. However, many applications of weld-bonded joints involve the possibility of dynamic fracture and fatigue loading. While the values of the cohesive parameters used in the current work may not be directly applicable to these other loading conditions, it is expected that cohesive-zone approaches should still be applicable. Various groups have addressed time- and cyclic-dependent effects on cohesive-zone models (Refs. 33–37). It is expected that these approaches could be adapted to model fatigue and time-dependent effects of welded and weld-bonded geometries.

Conclusions

Finite-element calculations incorporating cohesive-zone modeling have been shown to provide predictions for the deformation and fracture of weld-bonded

joints. Implementation of this method requires that two cohesive-fracture parameters, the peak stress and toughness, be specified for each mode of deformation in each potential region of fracture. In the current study, these parameters were determined from independent tests previously made on spot-welded and adhesively bonded joints. It has been shown that once the parameters have been established, they can be combined to predict the deformation and fracture of new weld-bonded joint geometries containing the identical spot weld and adhesive. Strengths, deformations, energy-absorption and failure modes are captured fairly accurately. The results presented in this paper indicate that the use of cohesive-zone models may have the potential to be a very useful approach for the design and analysis of weld-bonded joints.

Acknowledgments

The authors would like to thank R. Cooper of Ford Motor Co., Scientific Research Labs (SRL), for help with the spot welding machine as well as J. Hill, S. Ward, and K. Lasarz, also of Ford SRL, for providing the 5754 aluminum and XD4601 adhesive. Helpful conversations with K. Garikipati of the University of Michigan are gratefully acknowledged. M. N. Cavalli was partially supported by the National Science Foundation through a graduate fellowship and by the American Welding Society through a graduate fellowship research grant.

References

1. Irving, R. 1994. Weld bonding finds new applications on automotive assembly lines. *Welding Journal* 73(7): 41–42.

2. Ghosh, P. K., and Sambasivarao, N. 1998. Weld-bonding of thin sheet aluminum. *International Journal of Joining of Materials* 10: 45–53.

3. Hills, D. R., Parker, J. D., and Williams, N. T. 1995. The effect of increasing sample width on the strength of weld-bonded lap joints. *Key Engineering Materials* 99–100: 119–126.

4. Hills, D. R., Parker, J. D., and Williams, N. T. 1996. Effect of number of welds in spot-welded and weld-bonded arrays on static failure load of individual spotwelds and adhesive bond. *Ironmaking and Steelmaking* 23: 150–156.

5. Moniatis, G., Dorn, L., and ElSawy, A. 1986. A comparison between adhesive-bonding and weld-bonding of HSLA steel. *Proceedings of an International Conference on Trends in Welding Research*, Gatlinburg, Tenn., May 18–22.

6. ElSawy, A. H., Salama, A. S., and Nan, Z. B. 1986. A comparison between the spot-welding and weld-bonding of aluminum alloys. *Proceedings of an International Conference on Trends in Welding Research,* Gatlinburg, Tenn., May 18–22.

7. Renshaw, T., Wongwiwat, K., and Sarrantonio, A. 1983. Comparison of properties of joints prepared by ultrasonic welding and other means. *Journal of Aircraft* 20: 552–556.

8. Jones, T. B. 1995. Weld-bonding: The mechanisms and properties of weld-bonded joints. *Sheet Metal Industries* 72: 29–31.

9. Bassler, H. I., El-Sebakhy, I., and Malik, D. J. 1992. Weld-bonding of structural adhesives for body stiffening. *SAE Technical Papers*, #922118, pp. 39–55.

10. Ring-Groth, M., and Magnusson, C. 2000. The fatigue properties of weld-bonded stainless steel joints. *Journal of Advanced Materials* 32: 21–27.

11. Melander, A., Larsson, M., Stenslo, H., Gustavsson, A., and Linder, J. 2000. Fatigue performance of weld-bonded high-strength sheet steels tested in arctic, room temperature and tropical environments. *International Journal of Adhesion and Adhesives* 20: 415–425.

12. Wang, P. C., Chisholm, S. K., Banas, G., and Lawrence, F. V., Jr. 1995. The role of failure mode, resistance spot weld and adhesive on the fatigue behavior of weld-bonded aluminum. *Welding Journal* 74(2): 41-s to 47-s.

13. Chang, B. H., Shi, Y. W., and Dong, S. J. 1999. A study on the role of adhesives in weld-bonded joints. *Welding Journal* 78(8): 275-s to 279-s.

14. Chang, B. H., Shi, Y. W., and Dong, S. J. 1999. Comparative studies on stresses in weld-bonded, spot-welded and adhesive-bonded joints. *Journal of Materials Processing Technology* 87: 230–236.

15. Al-Samhan, A., and Darwish, S. M. H. 2003. Strength prediction of weld-bonded joints. *International Journal of Adhesion and Adhesives* 23: 23–28.

16. Lee, Y. L., Wehner, T. J., Lu, M. W., Morrissett, T. W., and Pakalnins, E. 1998. Ultimate strength of resistance spot-welds subjected to combined tension and shear. *Journal of Testing and Evaluation* 26: 213–219.

17. Lin, S. H., Pan, J., Wu, S. R., Tyan, T., and Wung, P. 2001. Failure loads of spot-welds under combined opening and shear static loading conditions. *International Journal of Solids and Structures* 39: 19–39.

18. Wung, P. 2001. A force-based failure criterion for spot-weld design. *Experimental Mechanics* 41: 107–113.

19. Wung, P., Walsh, T., Ourchane, A., Stewart, W., and Jie, M. 2001. Failure of spot welds under in-plane static loading. *Experimental Mechanics* 41: 100–106.

20. Cavalli, M. N., Thouless, M. D., and Yang, Q. D. 2003. Cohesive-zone modeling of the deformation and fracture of spot-welded joints. Manuscript submitted for publication.

21. Cavalli, M. N. 2003. Cohesive zone modeling of structural joint failure. Ph.D. dissertation. Ann Arbor, Mich., University of Michigan.

22. Needleman, A. 1987. A continuum model for void nucleation by inclusion debonding. *Journal of Applied Mechanics* 54: 525–531.

23. Tvergaard, V., and Hutchinson, J. W. 1992. The relation between crack growth resistance and fracture process parameters in elastic-plastic solids. *Journal of the Mechanics and Physics of Solids* 40: 1377–1397.

24. Tvergaard, V., and Hutchinson, J. W. 1996. On the toughness of ductile adhesive joints. *Journal of the Mechanics and Physics of Solids* 44: 789–800.

25. Roychowdhury, S., Arun Roy, Y. D., and Dodds, R. H., Jr. 2002. Ductile tearing in thin aluminum panels: Experiments and analyses using large-displacement, 3-D surface cohesive elements. *Engineering Fracture Mechanics* 69: 983–1002.

26. Yang, Q. D., Thouless, M. D., and Ward, S. M. 1999. Numerical simulation of adhesively bonded beams failing with extensive plastic deformation. *Journal of the Mechanics and Physics of Solids* 47: 1337–1353.

27. Yang, Q. D., Thouless, M. D., and Ward, S. M. 2000. Analysis of the symmetrical 90° peel test with extensive plastic deformation. *Journal of Adhesion* 72: 115–132.

28. Yang, Q. D., Thouless, M. D., and Ward, S. M. 2001. Elastic-plastic mode-II fracture of adhesive joints. *International Journal of Solids and Structures* 38: 3251–3262.

29. Yang, Q. D., and Thouless, M. D. 2001. Mixed-mode fracture analysis of plastically deforming adhesive joints. *International Journal of Fracture* 110: 175–187.

30. Kafkalidis, M. S., and Thouless, M. D. 2002. The effects of geometry and material properties on the fracture of single lap-shear joints. *International Journal of Solids and Structures* 39: 4367–4383.

31. Kafkalidis, M. S., Thouless, M. D., Yang, Q. D., and Ward, S. M 2000. Deformation and fracture of adhesive joints constrained by plastically deforming adherends. *Journal of Adhesion Science and Technology* 14: 1593–1607.

32. Standard E8M-99, 1999. *Standard Test Method for Tension Testing of Metallic Materials [Metric].* ASTM.

33. Nguyen, O., Repetto, E. A., Ortiz, M., Radovitsky, R. A. 2001. A cohesive model of fatigue crack growth. *International Journal of Fracture* 110: 351–369.

34. Roe, K. L., and Siegmund, T. 2003. An irreversible cohesive zone model for interface fatigue crack growth simulation. *Engineering Fracture Mechanics* 70: 209–232.

35. Landis, C. M., Pardoen, T., and Hutchinson, J. W. 2000. Crack velocity dependent toughness in rate dependent materials. *Mechanics of Materials* 32: 663–678.

36. Rahulkumar, P., Jagota, A., Bennison, S. J., and Saigal, S. 2000. Cohesive element modeling of viscoelastic fracture: application to peel testing of polymers. *International Journal of Solids and Structures* 37: 1873–1897.

37. Allen, D. H., and Searcy, C. R. 2001. A micromechanical model for a viscoelastic cohesive zone. *International Journal of Fracture* 107: 159–176.